BioCore
Exploring Scientific Community

International Journal of Nanotechnology in Medicine & Engineering

Research Article
ISSN 2474-8811

Photocatalytic Removal of Organic Pollutants from Industrial Wastewater Using MnO, NiO and Mixed MnO-NiO NP's as Catalyst

Islam M. I. Moustafa*, El - Sayed M. Mabrouk and Mona M. Ashraf

Chemistry Department, Faculty of Science, Benha University, Benha, Egypt

Abstract

Removal of malachite green dye (MG^+), organic pollutant, from wastewater was investigated by photocatalytic method using MnO, NiO and mixed MnO – NiO nano particles (NP's) prepared from different organic precursors as catalyst. The as – prepared nano oxides were characterized by different physicochemical techniques viz, thermal analysis, FTIR, HRTEM and X-Ray diffraction methods then their antibacterial and anticancer effects against Breast carcinoma MCF-7 cell line were studied. Three types of oxide NP's having sizes near to 50 nm were used to find the optimum conditions for photocatalytic degradation and removal of MG^+ from wastewater by studying the effect of various parameters on the degradation rate including the catalyst concentration, process duration as well as the catalytic effectiveness of the oxide NP's. In addition, the effect of UV light sources on the degradation process was studied. The process performed with the nanostructured oxides catalyst was very successfully allowing best degradation of organic compounds. The sorption kinetic and thermodynamic modeling was also studied

Keywords: MnO - NiO NP's, Antibacterial, Anticancer, Photocatalysis, MG^+ Pollutant

Corresponding author: **Islam M. I. Moustafa**

Chemistry Department, Faculty of Science, Benha University, Benha, Egypt, **Tel:** 0020201007535354

Email: islamshahin84@outlook.com

Citation: Islam M. I. Moustafa et al. (2019), Photocatalytic Removal of Organic Pollutants from Industrial Wastewater Using MnO, NiO and Mixed MnO-NiO NP's as Catalyst. Int J Nano Med & Eng. 4:6, 46-55

Received: September 13, 2019
Accepted: September 23, 2019
Published: November 11, 2019

Introduction

Nanotechnology is considered as having the potential to play an important role in shaping our current environment by providing new materials, remediation/treatment techniques and sensors for water purification. It has the ability to remove toxic contaminants from the environment to a safe level and to do so rapidly, efficiently and within a reasonable costs framework. Thus, the development of novel nanomaterials with increased affinity, capacity and selectivity for heavy metals and organic contaminants is an active emerging area of research in the field of nanotechnology. The benefits of using nanomaterials are mainly associated with their large specific surface area and high reactivity [1]. A variety of efficient, cost-effective and environmentally-friendly nanomaterials have been developed, each possessing unique functionality in their potential application to the detoxification of industrial effluents, groundwater and surface water. These nanomaterials have various applications in many scientific and industrial fields, including wastewater purification, catalysis and magnetic devices [2-5]

Malachite green (MG^+) also called aniline green, basic green 4, diamond green B or Victoria green dye, with IUPAC name 4 – [(4 - dimethylaminophenyl) – phenylmethyl] – N,N – dimethylaniline is a triphenylmethane dye and a derivative of bis (p – aminophenyl) phenylmethane . Its reduced form (leuco – malachite green) occurs as a contaminant in aquatic and terrestial ecosystem and is therefore potential human health hazards [6]. It is known as an antimicrobial agent [7] and therefore used as a preservative against fungal infection in fish [8], as dyes for fabric and paper [9] and as a cytochemical stain [10]. In the present study and in continuity to our researches on the preparation, characterization and application of simple and mixed nano oxides in the fields of biological activity and water purification [11 – 14], MnO, NiO and mixed MnO-NiO NP's were prepared starting from different organic precursors, characterized by thermal analysis, FTIR, HRTEM and X Ray diffraction tools then their antibacterial and anticancer effects against Breast carcinoma MCF-7 cell line were studied. The optimum conditions favoring the use of the as-prepared NP's as catalyst for the removal of MG+ from water sample were extensively studied.

Experimental

Materials and reagents

All chemicals used in the present study were of pure grade (Aldrich or Merck) and were used without further purification. Bi-distilled water was used all over the work. Manganese sulphate tetrahydrate ($MnSO_4.4H_2O$)(Merck), Nickel acetate hexahydrate ($Ni(CH_3COO)_2.6H_2O$) (Aldrich), oxalic acid ($H_2C_2O_4.2H_2O$), malonic acid, tartaric acid and citric acid (Aldrich) were used to prepare the precursors.

Preparation of the nanosized mono and mixed oxides

The hydrated acetate and sulphate salt of each of Ni2+ and Mn2+ (0.50 mol) was dissolved in 150 ml bidistilled water and titrated with 0.50 mol/150 mL of different organic acids (oxalic acid, malonic acid, tartaric acid or citric acid) with constant stirring tell complete precipitation. The precipitate was left in contact with the mother liquor for about 2 hours, filtered, washed several times by hot bidistilled water, dried at 120°C in an oven for 2 hours, then finally calcined at 600°C for 6 hours. For preparation of coubled MnO – NiO, binary mixtures of the hydrated acetate and sulphate salts of (Mn^{2+}, Ni^{2+}) in equal molar ratios were titrated with oxalic acid or tartaric acid with slow addition and continuous stirring for about 2 hours. After finishing titration, the precipitates so formed were treated as mentioned above.

Instruments and characterization methods

All the instruments used in this study were the same as described in our previous work [12].

Antimicrobial Screening

The antimicrobial susceptibility against Gram – positive bacteria (Streptococcus pyogenes and Staphylococcus epidermidis) and Gram – negative bacteria (Proteus vulgaris and Klebsiella pneumonia) was tested by the disk diffusion technique developed by Bauer et al[15] and described in our previous work [16]. The method is based on the determination of an inhibited zone proportional to the bacterial susceptibility to the antimicrobial present in the disk. Three replicas were made for each treatment to minimize error.

Antitumor activity assay.

In vitro anticancer activity evaluation of some selected nano particles was carried out against human cancer MCF-7 cell line using MTT method at The Regional Center for Mycology & Biotechnology, Al – Azhar University, Cairo, Egypt [17]. The 50% inhibitory concentration (IC_{50}) was estimated from graphic plots of the dose response curve for each concentration using Graphpad Prism software (San Diego, CA. USA) [18].

Photocatalytic degradation

The photocatalytic activity was evaluated by the decomposition of malachite green (MG^+) in aqueous solutions under UV irradiation. A 20 W UV lamp (λ = 253.7 nm) was used as light source with light intensity of 0.75 mW/cm2. The catalyst powders (20 mg) were added to 250 ml of MG^+ (30 mg/l). The distance between the liquid surface and the light source is kept at 10 cm and the solution was stirred for 5 min before irradiation. During the experiment the concentration of the dye was determined using a UV-Visible spectrophotometer at its maximum wavelength (618 nm). The percent photodegradation efficiency (%D) was calculated as:

$$\% D = (Co-Ct)/Co \times 100 \approx (Ao-At)/Ao \times 100$$

where C_o is the initial concentration of the dye solution and Ct is its concentration at time (t).

Results and Discussion

Preparation and characterization of oxide NP's

Manganese oxides NP's (M1 and M2) were prepared starting from manganese oxalate and manganese tartrate precursors, respectively. The NiO NP's (MA1 – MA4) were prepared from the oxalate (MA1), malonate (MA2), tartrate (MA3) and citrate (MA4) precursors while, the mixed oxides (MX1 and MX2) were prepared from mixture of oxalate (MX1) and tartrate (MX2) precursors. The organic salt precursors were dried at 120°C, and were characterized by elemental - thermal analysis and FTIR spectra before calcinated at 650°C to get the final nano oxides.

i- Thermogravimertic Analysis

The thermogravimetric-differential thermal analysis were performed on the organic acid precursors to follow their thermal decomposition to the final oxide forms. Example of the TG-DTA curves of manganese oxalate sample is shown in Fig.(1) and the data of thermal events are listed in Table (1). Inspection of the data obtained showed that the organic precursors degrade thermally in, more or less, three steps; the first at the temperature 43.55 - 156.86°C due to the dehydration of physically adsorbed or crystallinity water (this step is sometimes a composite of two steps). The beginning of the thermal degradation of the unhydrous compounds took place within the second step at the temperature range of 221.49 – 276.2°C by the evolution of gases such as N2 and/or CO_2. Complete decomposition of the organic precursors occurred in the third step within the range 341.92 – 375.5°C which led to the formation of the nanosized metal oxides as final products.

Compound	Temp.(°C)	Assignment
Mn- oxalate (M1)	128.66 (s) 310.36 (s) 460.04 (w) 829.95 (m)	Removal of physically adsorbed H_2O Removal of water of crystallization Decomposition of unhydrous Mn-oxalate
Mn- tartrate (M2)	142.83 (m) 247.45 (s) 354.60 (w) 817.20 (w)	Removal of physically adsorbed H_2O Removal of water of crystallization Decomposition of unhydrous Mn – tartrate
Ni- oxalate (MA1)	208.89 (s) 319.69 (s)	Dehydration process Decomposition to NiO NP
Ni – malonate (MA2)	43.55 (m) 221.49 (s) 341.92 (s)	Removal of physically adsorbed H_2O Removal of water of crystallization Decomposition of unhydrous Ni – malonate
Ni- tartaratae (MA3)	156.86 (m) 232.14 (s) 349.11 (s)	Removal of physically adsorbed H_2O Removal of water of crystallization Decomposition of unhydrous Ni – tartrate

Table 1: Thermogravimetric data for the Mn and Ni – organic acids precursors.

Ni- citrate (MA4)	241.89 (s) 276.20 (w) 865.12 (w)	Removal of physically adsorbed H_2O Removal of water of crystallization Decomposition of unhydrous Ni – citrate
Mn – Ni oxalate (MX1)	83.00 (w) 375.50 (s)	Dehydration process Decomposition to MnO - NiO NP
Mn – Ni tartarate (MX2)	57.92 (w) 133.27 (m) 313.57 (m) 367.36 (s)	Removal of physically adsorbed H2O Removal of water of crystallization Decomposition of unhydrous Mg-salt of glycine

Table 1: Thermogravimetric data for the Mn and Ni – organic acids precursors.

The thermogravimeteric – differential thermal studies were performed on the organic acid precursor after ignition at 650°C (the oxide samples). Example of the obtained thermograms is shown in Fig. (2). From the study it was noted that the thermograms show no any thermal events up to ≈ 850°C where a weak endothermic peaks were obtained. This is due to the transformation of Mn_3O_4 to MnO [19] and Ni (II) oxide to Ni2O3 and/or NiO_2 [20] according to the equations:

$$2Mn_2O_3 \rightarrow 4MnO + O_2, \quad 2NiO + 4/3O_2 \rightarrow Ni_2O_3 \text{ and } \quad NiO + 1/2O_2 \rightarrow NiO_2$$

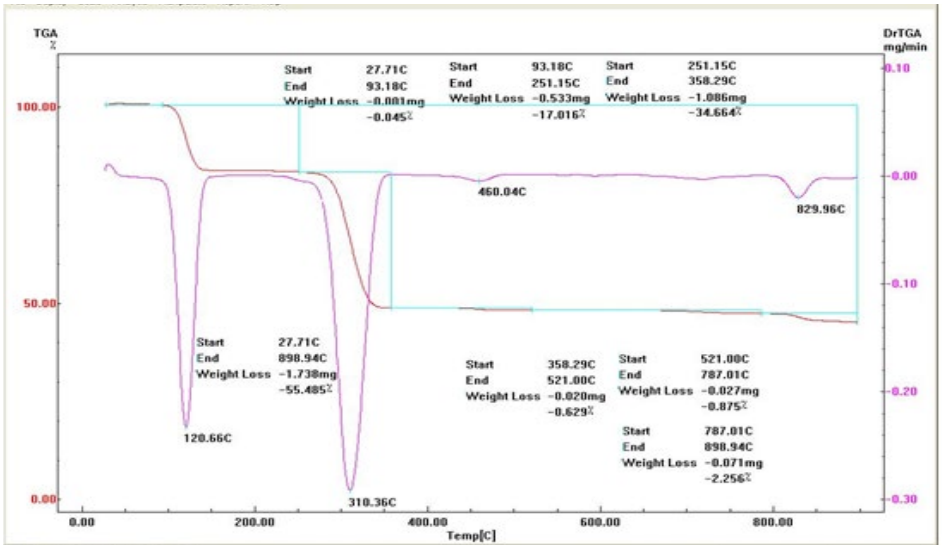

Fig 1: TGA – DtA curves for Mn oxalate precursor

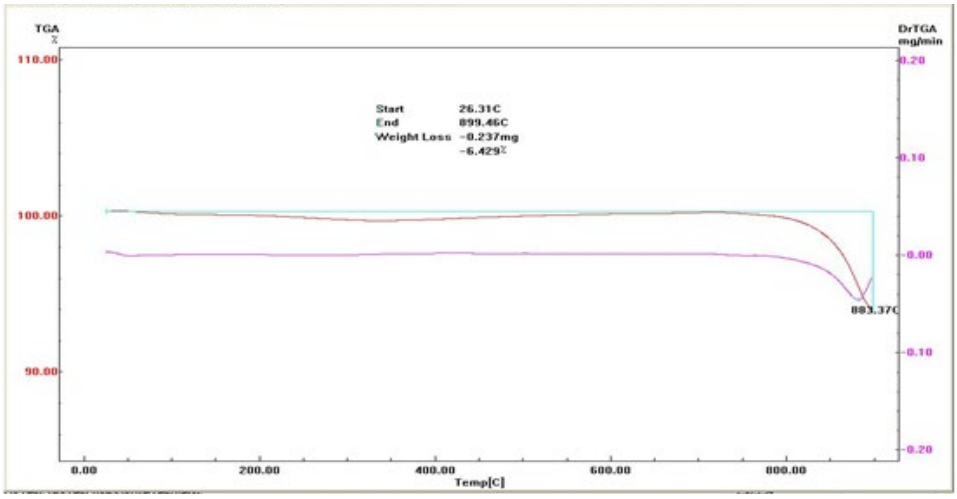

Fig: 2: TGA – DtA curves for Mn oxalate precursor after ignition at 650°C

FTIR spectra of the as-prepared metal nanooxide were scanned and compared to those of the organic precursors before ignition. The spectra of the latter showed the vibrational frequencies of the functional groups (ν_{OH}, $\nu_{C=O}$, ν_{COO} , δ_{OH}, and ν_{O-M}) as shown in Table (2). The FTIR spectra of the organic acids precursors show broad absorption bands within the wavenumber ranges 3120 - 3385 cm-1 and 925 - 1237 cm^{-1} due to the stretching and bending vibrations of the trace water molecule, respectively. The two bands within the range 1623 – 1744 cm^{-1} and 1291 - 1410 cm^{-1} are due to the stretching vibrations of C=O and (V_{COO}) bonds, respectively. These bands are, more or less, disappeared in case of calcinated samples. In the spectra of the nanooxides, the weak broad band at ≈ 3350 cm^{-1} is due the stretching vibration of the ν_{OH} group of physically adsorbed water molecule on the surface while the weak bands within the rangr 925 - 1096 cm^{-1} are due to δOH bending vibrations mode. The IR spectra of metal oxides NP's exhibit the characteristic absorption bands in the shortwave region around 500 cm^{-1} due to νM-O stretching frequencies. It is worthy to mention that there is a shift in the IR active mode, which is due to nano size grain. For a nano size grain, the atomic arrangement on the boundaries differ greatly from that of the bulk crystals, both in coordination number and bond lengths, showing some extent of disorder[21] Crystal symmetry is thus, degraded in nano size grains. The degradation in crystal symmetry results in the shifting of the IR active mode[22].

Compound	IR frequency (cm^{-1})				
	ν_{OH}	$V_{C=O}$	ν_{COO}	δ_{OH}	M – O
Mn- acetate	3385.5	1627.8	1313.8	1140.4	506.2
MnO (M1)	--	--	--	--	524.5
Mn- tartrate	3360.8	1744.2	1327.8	1148.8	517.6
MnO (M4)	---	---	---	---	570.4
Ni- oxalate	3392.7	1659.8	1360	1316.6	628.2
NiO (MA1)	---	---	---	---	481.55
Ni – tartrate	3120.2	1601.1	1401.1	925.1	509.1
NiO (MA3)	---	---	---	---	675.5
Mn – Ni oxalate	3381.9	1623.7	1360.5	1314.7	812.8 - 743.4
(MnO-NiO (MX1)	---	---	---	1453.9	600.6 – 510.1
Mn – Ni tartarate	3412	1743.7	1291.4	1237	687.1 - 551.6
(MnO-NiO (MX2)	---	---	---	1096.8	598.4– 437.7

Table 2: IR frequencies (cm^{-1}) of some important groups for selected organic acids precursors and the corresponding nanooxide.

X-Ray Diffraction Analysis (XRD)

The X-ray diffraction patterns of the nano sized manganese oxide (M2), nickel oxide (MA4) and Mn-Ni mixed oxides (MX1 and MX2) prepared by co-precipitation method are shown in Fig.(3). The XRD studies reveal that the nanoparticles of these oxides are crystalline. The relative crystalline sizes were determined from the XRD lines broadening using the Scherrer equation [23] using computer program. From calculation, the average crystalline size was found to be 50.81 nm, 42.4 nm, 42.1. nm and 47.32 nm for manganese oxide (M2), nickel oxide (MA4), Mn – Ni oxide (MX1) and Mn – Ni oxide (MX2) respectively. The phase purity of all the four samples was established by comparison of the X-ray diffraction patterns with JCPDS international data value. Manganese oxide was in matching with card No. #73-1704 and nickel oxide with # 78-0423.

The XRD pattern of the manganese oxide shows the presence of mixed phases of manganese oxides; Mn_2O_3 (orthorhombic with a=9.41, b=9.42 and c= 9.42) and Mn5O8 (monoclinic with a= 10.35, b= 5.72 and c= 4.85). while, the XRD pattern of the nanosized NiO, compared to XRD standard table, shows diffraction peaks corresponding to crystallographic planes (111), (200), (220) and (311) indicating pure NiO particles (hexagonal with a=b= 2.954 and c= 7.24).

In the mixed oxides diffractometer, the angle (d-spacing) and the intensities of the high angle reflected beam serve as a finger print of the crystal structure. The most intense peak (intensity 100) is from the (311) and (111) plane which corresponds to an angle of 2θ = 26.27° and 43.37° for manganese and nickel oxides, respectively. The XRD peaks are broadened due to the nano crystalline nature of the particles

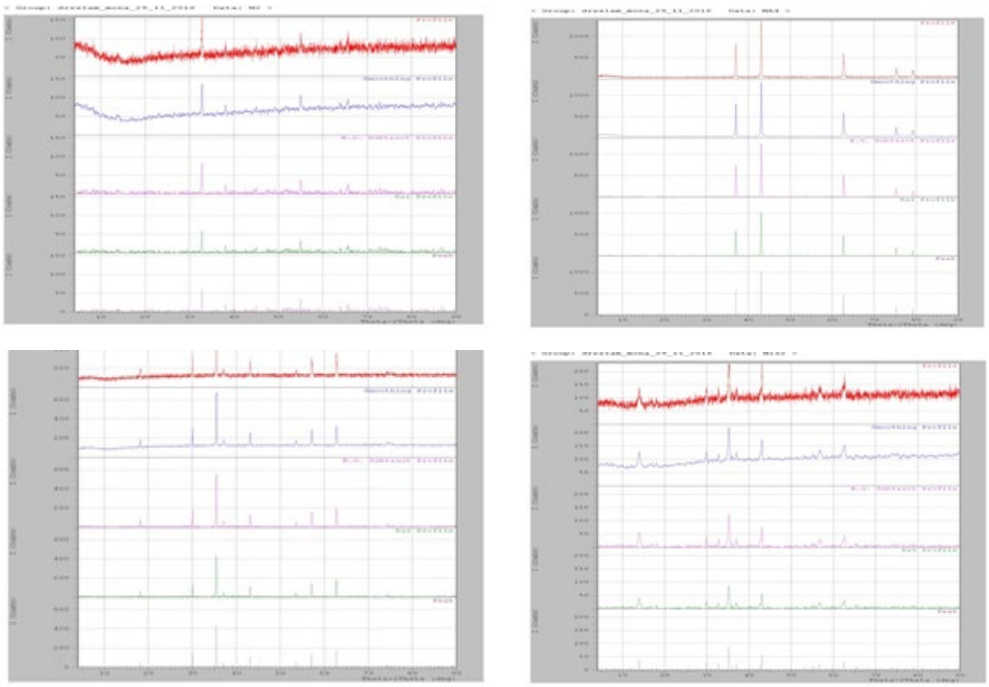

Fig 3: X Ray diffraction pattern for (M2), (MA4), (MX1) and (MX2) Np's.

High Resolution Transmission Electron Microscopy (HRTEM)

The micro structural analysis of the as synthesized samples calcined at 650°C for 6 hours was investigated using HRTEM. The TEM images are shown in Fig.(4). It can be seen from the graphs that manganese nanoparticles have narrow size distribution and are rectangular rode shapes with weak agglomeration. The HRTEM images for nickel oxide showed that the particles have square shape with size ranging from 24.64 to 31.75 nm and there is no agglomeration in the particles of the nano crystal

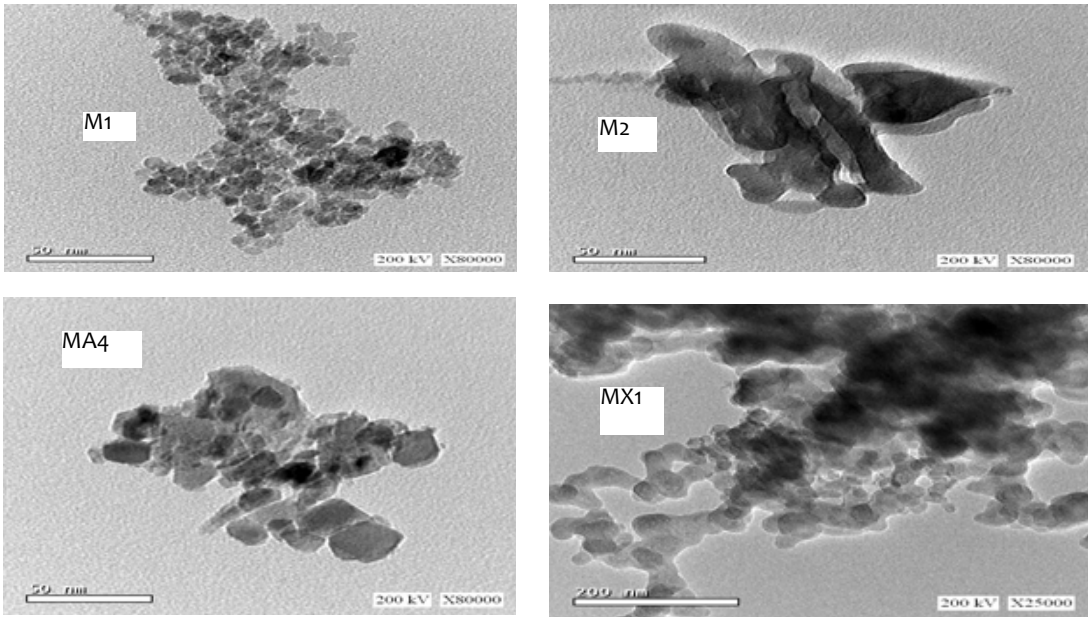

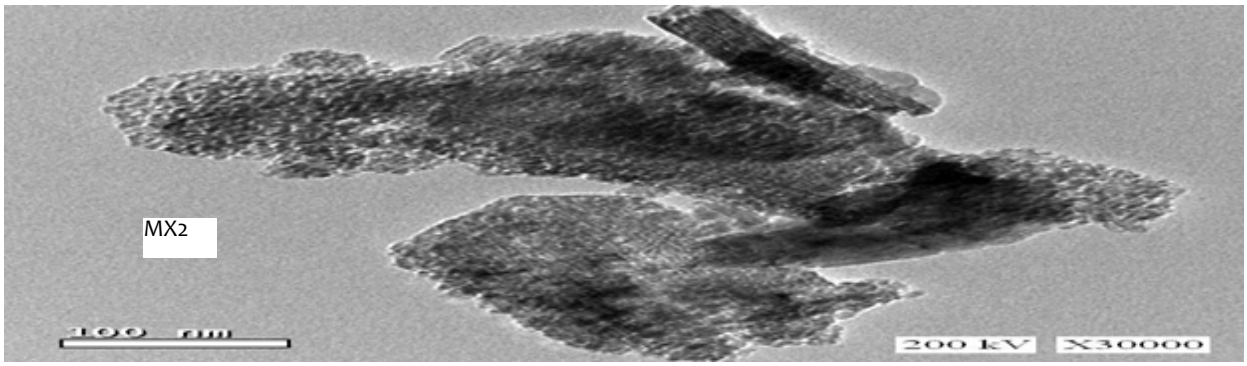

Fig 4: HRTEM for (M1), (M2), (MA4), (MX1) and (MX2) NP's

Biological Applications

Antimicrobial activity

The antimicrobial activity of some oxide NP's was tested against representatives of Gram – positive bacteria (Streptococcus pyogenes and Staphylococcus epidermidis) and Gram – negative bacteria (Proteus vulgaris and Klebsiella pneumonia). Standard drug; levofloxacin and DMF solvent control were screened separately for their antibacterial activity. The antibacterial results (c.f. Table 4) suggest that the as prepared nanooxides show high activity against the tested organisms. Although there is no general trend concerning the antimicrobial effect of the tested samples, but the activity is, more or less, in the order mixed Mn – NiO >NiO> MnO. The positive results suggest the diffusion of the nano particles into the lipid layer of the cell membrane of bacteria making them able to kill the bacterium as indicated by the zones of inhibition of bacterial growth.

Organism	Strept. Pyog			Staph. Epid			Prot. Vulgaris			Kleb. Pne		
Conc. (µg/mL)	5	10	20	5	10	20	5	10	20	5	10	20
Levofloxacine	**12**	**16**	**22**	**15**	**18**	**25**	**12**	**15**	**25**	**15**	**18**	**25**
M1	10	13	22	14	14	20	11	13	22	14	20	27
M2	12	14	20	16	14	21	12	13	23	13	14	20
MA1	12	15	20	12	14	22	14	14	25	17	20	26
MA3	13	13	18	14	17	22	12	13	20	14	16	21
MX1	14	15	22	14	20	24	11	13	25	16	17	26
MX2	14	14	24	15	18	24	12	16	24	14	18	25

Table 3: Inhibition zone diameter (mm) of levofloxacin and the metal oxides NP against various microorganisms

Antitumor activity

The cytotoxic activities of some selected nano oxides were tested against Breast carcinoma MCF-7 cell line and compared to that of Vinblastine as a standard drug. The relation between surviving cells and NP's concentration is plotted to get the survival curve of each tumor cell line after treatment with the nanooxide particles. The 50% inhibitory concentration (IC_{50}) was estimated from graphic plots of the dose response curve for each concentration. An example of the survival cure is shown in Fig. (5) while the lethal concentrations (IC_{50}) values compared to that of the standard Vinblastine drug are listed in Table (5). Inspection of the cytotoxic data, it is found that Ni NP (MA2) prepared from malonate precursor is the most effective among the rest oxides. In general, the cytotoxicity efficiency is in the order NiO (MA2)> MnO (M2) Mn-Ni mixed oxide (MX2)> NiO (MA4) > Mn-Ni mixed oxide (MX1). The enhanced activity of nano metaloxides may be attributed to the increase in penetrating process taking place through the cell lines.

Compound	Precursor	IC_{50} (µg/mL)
Vinblastine	…..	4.6
(MnO) M2	Tartrate	424
(NiO) MA2	Malonate	405
(NiO) MA4	Citrate	445
Mn – Ni Oxide MX1	Acetate	471
Mn – Ni Oxide MX2	Tartrate	440

Table 4: Lethal concentration (IC_{50}) of the as prepared nano oxide against MCF-7 cell line

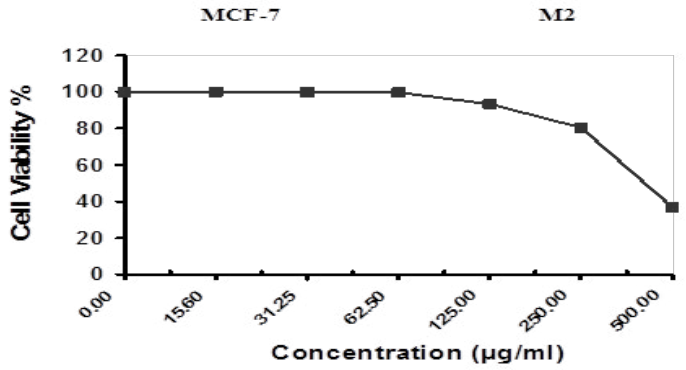

Fig 5: Cytotoxicity effect of nanooxide M2 against MCF-7 cell line

Analytical Application

Photocatalytic activity

Nanosized manganese oxide (M2), nickel oxide (MA4) and mixed manganese - nickel oxide (MX1) were tested as catalyst for the photodegradation of MG^{+} under UV irradiation. The absorption spectra of the dye were recorded after different time intervals (c.f. Fig.6 as an example). It was found that while MG degraded up to ≈ 48.2% in absence of catalyst after 120 min, the degradation efficiency increased to 86.6% and 80.7% on using the nanosized oxide M2 and MA4, respectively as catalyst after the same time (Fig. 7 as example).

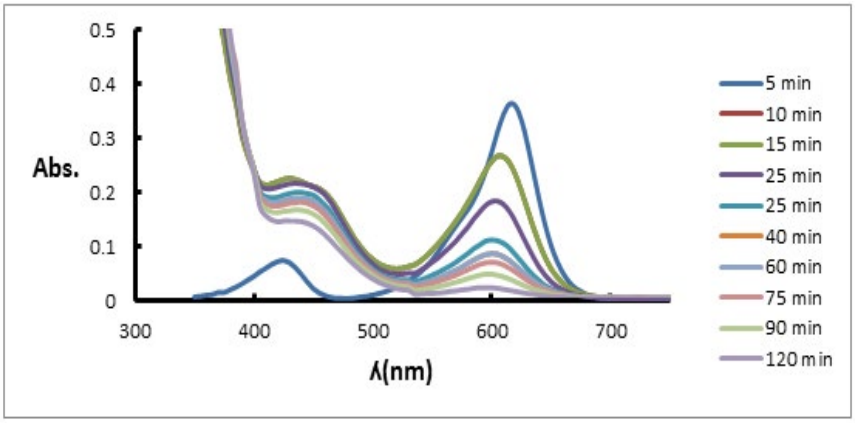

Fig 6: Effect of time on the removal of MG^{+} using M2 as catalyst

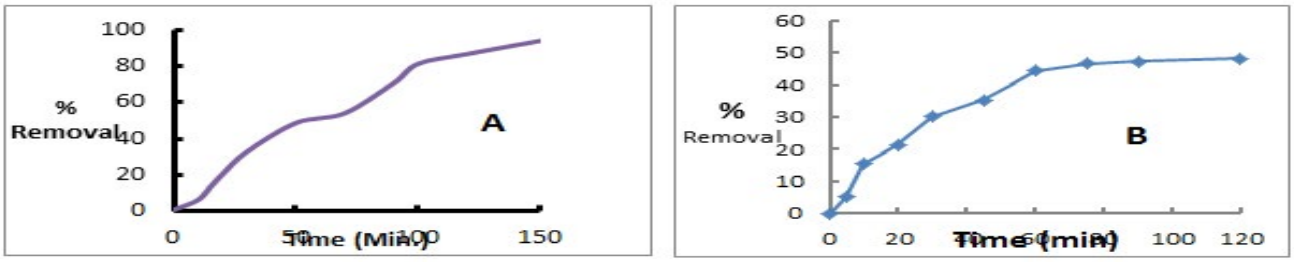

Fig 7: Effect of time on the % removal of MG using M2 as catalyst (A) and without catalyst (B).

The photodegradation efficiency, on using the mixed nanoparticle oxide MX1 as a catalyst is higher than those obtained in case of mono oxides NP's. It reaches about 90.2% after 60 min. compared to 48.2 % in absence of catalyst.

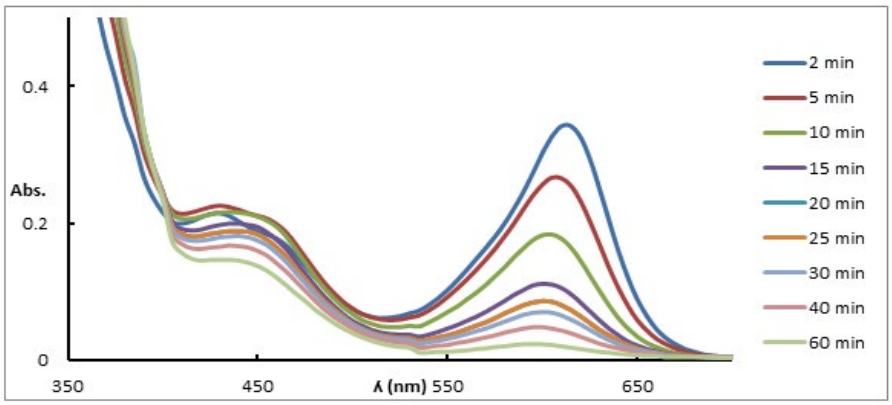

Fig 8: Effect of time on the degradation of MG^{+} using MX1 as sorbent Sorption kinetic modeling

Pseudo – first order and pseudo – second order rate equations were applied to analyze the adsorption kinetics of MG from wastewater onto NP's surface at 25±1°C. The linear form of the pseudo – 1st order kinetic model is given by the equation:

$$\log(qe - qt) = \log qe - \frac{k1}{2.303}t \qquad (1)$$

Where K1 is the pseudo 1st order rate constant (min-1), qe and qt (mg/g) are the amount of adsorbed dye at equilibrium and at time t (min), respectively. The values of these constants are calculated from the slope and intercept of the linear relation between log ($q_e - q_t$) and t (c.f.Fig.9).

The linearized form of pseudo – second order model is given by:

$$\frac{t}{q_t} = \frac{1}{k_2 q_e^2} + \frac{1}{q_e}(t) \qquad (2)$$

Where k2 is the rate constant of the 2nd order equation calculated from the slope of the linear relation between t/qt and t (c.f.Fig.10).

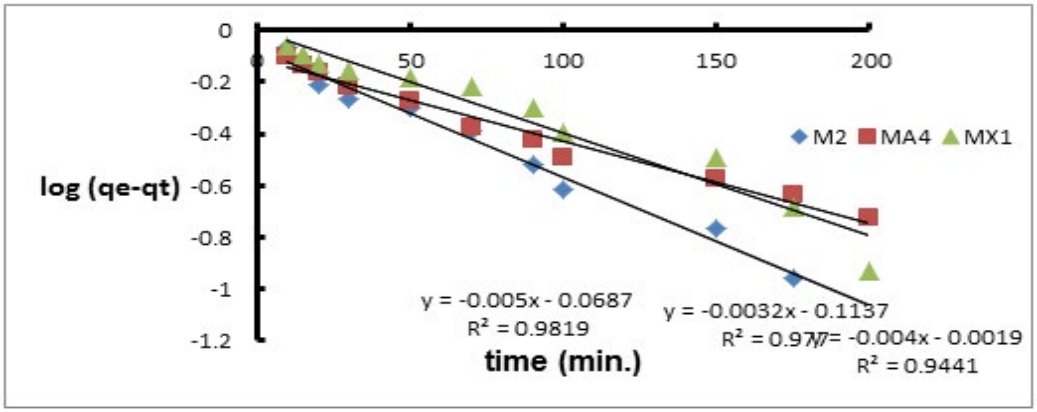

Fig 9: Pseudo 1st relations for the catalysts M2, MA4 and MX1

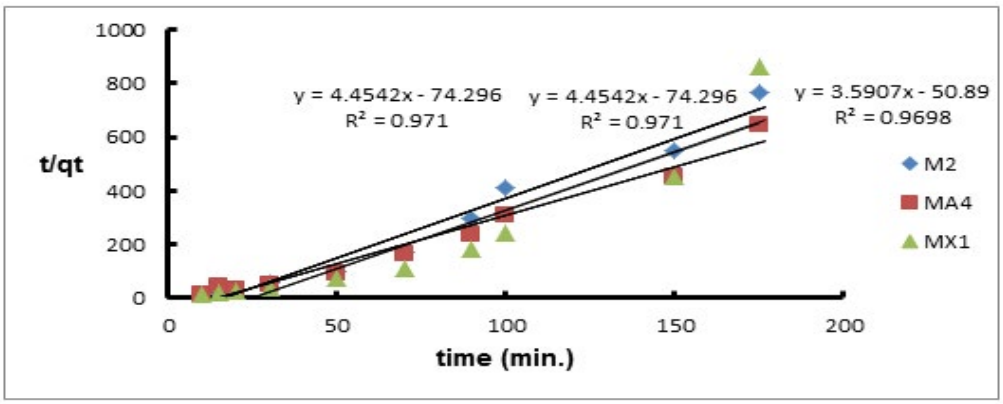

Fig 10: Pseudo 2nd relations for the catalysts M2, MA4 and MX1

The sorption kinetic data are cited in Table (6) from which it is clear that the pseudo first order model is the better applicable

Calculation of the thermodynamic activation parameters

Enthalpy of activation, ΔH*, and entropy of activation ΔS*, were calculated using transition state theory equation (Eyring Equation)

$$k = \frac{KT}{h} \exp\left(\frac{\Delta S^*}{R}\right) \exp\left(-\frac{\Delta H^*}{RT}\right)$$

where : K is the Boltzman constant, h is the Plank's constant, R is the universal gas constant, and T is the absolute temperature. Taking the natural logarithms

$$\ln\frac{k}{T} = \ln\left(\frac{K}{h}\right) + \frac{\Delta S^*}{R} - \frac{\Delta H^*}{RT}$$

A plot of ln (k / T) against 1 / T is linear (Fig. 11), with a slope equal (- ΔH^* / R) and intercept (ln K / h + ΔS^* / R). Therefore, ΔH^* and ΔS^* can be calculated from the slope and intercept, respectively. The thermodynamic parameter; free energy change ΔG is calculated using the equation: ΔG = ΔH - TΔS and are given in Table (6).

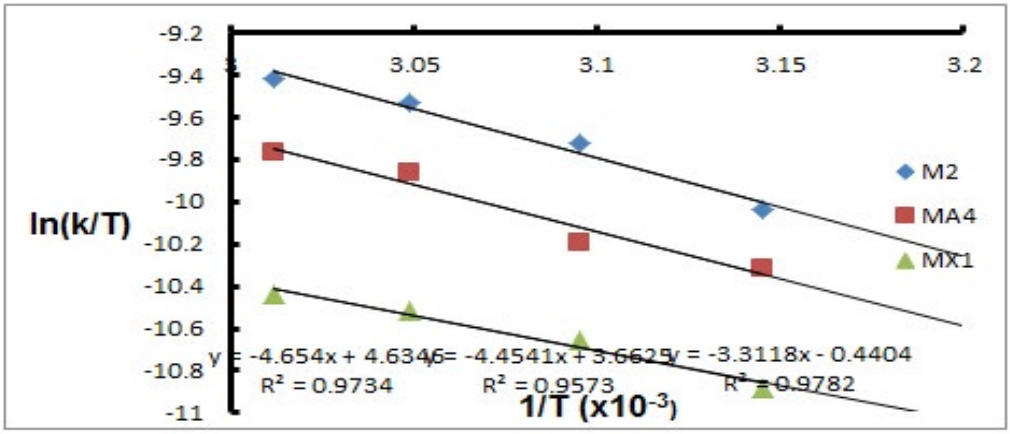

Fig 11: Relation between ln(K/T) and 1/T for the catalysts M2, MA4 and MX1

Catalyst	Pseudo 1st order		Pseudo 2nd order			Thermodynamic parameters		
	K1	R^2	K_2	q_e	R^2	ΔH	ΔS	ΔG
M2	0.0115	0.9819	0.266	0.225	0.9770	38.70	-131.62	-39.18
MA4	0.0074	0.9770	0.266	0.225	0.977	37.03	-148.00	-44.07
MX1	0.0092	0.9441	0.257	0.279	0.9698	27.54	-174.77	-52.05

Table 5 : Kinetic and thermodynamic parameters for the catalysts M2, MA4 and MX1

References

1. S. Singh, K. C. Barick and D. Bahadur; J. Nanomaterials and nanotechnology, 3, (11), (2013).
2. M. F. Abdel-Messih, M. A. Ahmed and A. S. El-Sayed; J. Photochemistry and Photobiology (A): Chemistry, 260, (2013),1-8
3. M .A. Gondal, M. M. Khaled, S. Ahmed and A. M. Shemsi; Appl. Catal. (A): General, 393,(1–2), (2011), 122-129
4. S. A. Hosseini, A. Niaei, D. Salari and S. R. Nabavi; Ceramics International, 38, (2),(2012),1655-1661
5. M. Batool, Z. Qureshi, N. Mehboob and A. Shah; Archives of Nanomedicine: Open Access Journal (ANOAJ), 1 – (4), (2018) .
6. Thomas Gessner and Udo Mayer "Triarylmethane and Diarylmethane Dyes" in Ullmann's Encyclopedia of Industrial Chemistry, 2002, Wiley-VCH, Weinheim.doi:10.1002/14356007.a27_179
7. S. Srivastava, R. Sinha and D. Roy; Aquatic Toxicology. 66 (3), (2004) 319–29.
8. C. W. Andersen, S. B. Turnipseed, and J.E. Roybal ; J. Agric. Food Chem., 54, (2006) ,4517–4523.
9. "Veterinary Residues Committee. Annual Report on Surveillance for Veterinary Residues in Food in the UK for 2001, 2002, and 2003" Archived 2012-02-11.
10. S. J. Culp, F. A. Beland and R. H. Heflich ; Mutation Research. 506–507, (2002), 55–63.
11. I. S. Ahmed, M. Y. Nassar, G. O. El-Sayed, H. A. Dessouki and Islam M. Ibrahim; Egypt. J. Appl. Sci. 28(6B), (2013), 366-375.
12. Islam M. Ibrahim , Moustafa E. Moustafa, Mohamed R. Abdelhamid, Journal of Molecular Liquids 223 (2016) 741–748
13. Islam MI Moustafa, Ihab A Saleh and Mohamed R Abdelhamid, J Material Sci Eng, 6(4), (2017), 1-8.
14. Islam M. I. Moustafa and Mohamed R Abdelhamid; J Chem Eng Process Technol, (2018) 9 – 1(DOI: 10.4172/2157-7048.1000372)
15. A. W. Bauer , W. M. Kirby , J. C. Sherris ,M. Turck ; Am. J. Clin Pathol 45, (1966), 493–496
16. I. M. I. Moustafa , H. E. Megahed andT. S. A. El-Baddally.; Advance Research Journal of Multidisciplinary Discoveries.29(5)(2018), 21-31
17. S. M. Gomha, S.M. Riyadh, E. A. Mahmmoud, and M. M. Elaasser; Heterocycles; 91(6), (2015), 1227-1243.
18. T. Mosmann; J. Immunol. Methods; 65, (1983), 55-63.
19. D. Devadatha and R. Raveendran ; J. Mater. Sci. Eng. (2013), special issue S:11
20. N. N. Greenwood and A. Earnshaw "(1984). Chemistry of the Elements. Oxford" Pergamon Press. (1984), 1336–37. ISBN 978-0-08-022057-4
21. J. Lu, H. Yang, B. Lui and G. Zou; Scripta Mater. Res. Bul, 34(1999), 2109.
22. M. Jose, K. Siby, M. Thomas and K. George; Ind, J. Pure Appl.Phys, 42 (2004), 121.
23. H. P. Klug and L. A. Alexnder "X-Ray powder diffraction procedure" John Wiley & Sons, New York (1954) p.184.